Conserved number fluctuations in a hadron resonance gas model

P. Garg[a], D. K. Mishra[b], P. K. Netrakanti[b], B. Mohanty[c], A. K. Mohanty[b], B. K. Singh[a], N. Xu[d,e]

[a] *Department of Physics, Banaras Hindu University, Varanasi 221005, India*
[b] *Nuclear Physics Division, Bhabha Atomic Research Center, Mumbai 400094, India*
[c] *School of Physical Sciences, National Institute of Science Education and Research, Bhubaneswar 751005, India*
[d] *Nuclear Science Division, Lawrence Berkeley National Laboratory, Berkeley, CA 94720, USA*
[e] *Key Laboratory of the Ministry of Education of China, Central China Normal University, Wuhan, 430079, China*

arXiv:1304.7133v1 [nucl-ex] 26 Apr 2013

Abstract

Net-baryon, net-charge and net-strangeness number fluctuations in high energy heavy-ion collisions are discussed within the framework of a hadron resonance gas (HRG) model. Ratios of the conserved number susceptibilities calculated in HRG are being compared to the corresponding experimental measurements to extract information about the freeze-out condition and the phase structure of systems with strong interactions. We emphasize the importance of considering the actual experimental acceptances in terms of kinematics (pseudorapidity (η) and transverse momentum (p_T)), the detected charge state and effect of resonance decays before comparisons are made to the theoretical calculations. In this work, based on HRG model, we report that the net-baryon number fluctuations are least affected by experimental acceptances compared to the net-charge and net-strangeness number fluctuations.

Keywords: , Hadron Resonance Gas, Susceptibilities, Higher moments, fluctuations, Heavy-ion collisions, critical point
PACS: 25.75.Bh, 25.75.Ld

1. Introduction

Measurement of the moments of distribution for conserved quantities like net-baryon, net-charge, and net-strangeness number for systems undergoing strong interactions as in high energy heavy-ion collisions, have recently provided rich physics insights [1, 2, 3, 4, 5, 6, 7, 8, 9, 10]. The most crucial realization is that, the product of moments of the conserved number distributions are measurable experimentally and can be linked to susceptibilities (χ) computed in Quantum Choromodynamic (QCD) based calculations [1, 5]. For example, $S\sigma = \chi^{(3)}/\chi^{(2)}$ and $\kappa\sigma^2 = \chi^{(4)}/\chi^{(2)}$, where σ is the standard deviation, S is the skewness, κ is the kurtosis of the measured conserved number distribution, $\chi^{(n)}$ are the n^{th} order theoretically calculated susceptibilities associated with these conserved numbers. Such a connection between theory and high energy heavy-ion collision experiment has led to furthering our understanding about the freeze-out conditions [2, 4], details of the quark-hadron transition [1, 8] and plays a crucial role for the search of possible QCD critical point in the QCD phase diagram [5]. In all such physics cases there is a need to establish a reference point for the measurements. Computing these quantities within the framework of a hadron resonance gas (HRG) model [11] provides such a reference for both experimental data and QCD based calculations.

The experimental measurements have limitations, they are usually available for a fraction of the total kinematic phase space, due to the finite detector geometries and can detect only certain species of the produced particles. For example, measurements related to net-baryon number distribution is restricted by the kinematic range in p_T where their identification is possible. In addition baryons like neutron are not commonly measured in most of the high energy heavy-ion collision experiments. While for the net-charge number distribution, the limitation is usually in kinematic range available in η and the details of how contribution from different charge states and resonances are dealt with in the measurements. The kinematic acceptance in a typical high energy heavy-ion collision experiment like STAR [12] and PHENIX [13] at the Relativistic Heavy-Ion Collider facility (RHIC) for net-charge multiplicity distributions are: $|\eta| < 0.5$, $0.2 < p_T < 2.0$ GeV/c and $|\eta| < 0.35$, $0.3 < p_T < 1.0$ GeV/c, respectively. While for net-baryon number and net-strangeness related studies carried out in the STAR experiment, within $|\eta| < 0.5$, is through the measurement of net-protons and net-kaons in the range of $0.4 < p_T < 0.8$ GeV/c and $0.2 < p_T < 2.0$ GeV/c, respectively [5, 12].

The main goal of this paper is to demonstrate using the HRG model (discussed in next section), the effect of the above experimental limitations on the physics observables $\chi^{(3)}/\chi^{(2)}$ and $\chi^{(4)}/\chi^{(2)}$. Our model based study clearly shows that the value of the observables related to net-charge and net-strangeness strongly depends on the experimental kinematic and charge state acceptances. Where charge state could be electric charge (Q) = 1 or higher for net-charge measurements and strangeness number (S) = 1 or higher for net-strangeness measurements. In contrast, the net-baryon number studies are found to be minimally affected by these experimental limitations.

The paper is organized as follows. In the Section 2, we will discuss the HRG model used in this study. In the Section 3, the results for the observable $\chi^{(3)}/\chi^{(2)}$ and $\chi^{(4)}/\chi^{(2)}$ are presented

Email address: bedanga@rcf.rhic.bnl.gov (B. Mohanty)

for different kinematic acceptances, charge states, and resonance decay contributions. We also provide a table listing the values of these observable for typical experimental conditions as encountered in STAR and PHENIX experiments at RHIC and ALICE experiment at the Large Hadron Collider (LHC) Facility. Finally in Section 4, we summarize our findings and mention about the implications of this work to the current experimental measurements in high energy heavy-ion collisions.

2. Hadron Resonance Gas Model

In the HRG model, we include all the relevant degrees of freedom of the confined, strongly interacting matter and also implicitly takes into account the interactions that result in resonance formation [3]. The logarithmic of the partition function (Z) in the HRG model within the ambit of a grand canonical ensemble framework is given as,

$$\ln Z(T,\mu_B,\mu_Q,\mu_S) = \sum_B \ln Z_i(T,\mu_B,\mu_Q,\mu_S) + \sum_M \ln Z_i(T,\mu_Q,\mu_S)\,, \quad (1)$$

where, $\ln Z_i(T,V,\mu) = \pm\frac{Vg_i}{2\pi^2}\int \partial^3k \ln\left\{1 \pm \exp(\mu - E)/T\right\}$, T is the temperature, V is the volume of the system, μ_i is the chemical potential and g_i is the degeneracy factor of the i^{th} particle. The total chemical potential $\mu = B\mu_B + Q\mu_Q + S\mu_S$, where B, Q and S are the baryon, electric charge and strangeness number of the i^{th} particle, with corresponding chemical potentials μ_B, μ_Q and μ_S, respectively. The '+' and '-' signs are for baryons and mesons respectively.

The thermodynamic pressure (P) can then be deduced for the limit of large volume as

$$\frac{P}{T^4} = \frac{1}{VT^3}\ln Z_i = \pm\frac{g_i}{2\pi^2T^3}\int \partial^3k \ln\left\{1 \pm \exp(\mu - E)/T\right\}. \quad (2)$$

The n^{th} order generalized susceptibility for baryons can be expressed as,

$$\chi^{(n)}_{x,baryon} = \frac{X^n}{VT^3}\int \partial^3k \sum_{m=0}^{\infty}(-1)^m(m+1)^n exp\left\{\frac{-(m+1)E}{T}\right\}exp\left\{\frac{(m+1)\mu}{T}\right\}, \quad (3)$$

and for mesons,

$$\chi^{(n)}_{x,meson} = \frac{X^n}{VT^3}\int \partial^3k \sum_{m=0}^{\infty}(m+1)^n exp\left\{\frac{-(m+1)E}{T}\right\}exp\left\{\frac{(m+1)\mu}{T}\right\}. \quad (4)$$

The factor X represents either B, Q or S of the i^{th} particle depending on whether the computed χ_x represents net-baryon, net-electric charge or net-strangeness susceptibility. Here $\partial^3k = p_T\sqrt{{p_T}^2 + m^2}\cosh\eta\ \partial p_T\ \partial\eta\ \partial\phi$ and $E = m_T\cosh\eta = \sqrt{{p_T}^2 + m^2}\cosh\eta$. Where m is the mass of the hadron and ϕ is the azimuthal angle of the produced hadron. The experimental acceptances can be incorporated by considering the appropriate integration ranges in η, p_T, ϕ and charge states by considering the values of $|X|$. The total generalized susceptibilities will then be the sum of the contribution from baryons and mesons as, $\chi^{(n)}_x = \chi^{(n)}_{x,baryon} + \chi^{(n)}_{x,meson}$.

In order to make the connection with the experiments, the beam energy dependence of μ and T parameters of the HRG model needs to be provided. These are extracted from a statistical thermal model description of measured particle yields in the experiment at various $\sqrt{s_{\rm NN}}$ [14, 15, 16]. This is followed by the parameterization of μ_B and T as a function of $\sqrt{s_{\rm NN}}$ [14, 16]. The μ_B dependence of the temperature is given as $T(\mu_B) = a - b\mu_B^2 - c\mu_B^4$ with $a = 0.166 \pm 0.002$ GeV, $b = 0.139 \pm 0.016$ GeV^{-1}, and $c = 0.053 \pm 0.021$ GeV^{-3}. The $\sqrt{s_{\rm NN}}$ dependence of μ_B is given as $\mu_B(\sqrt{s_{NN}}) = \frac{d}{1+e\sqrt{s_{NN}}}$ with $d = (1.308 \pm 0.028)$ GeV and $e = (0.273 \pm 0.008)$ GeV^{-1}. Further the ratio of baryon to strangeness chemical potential is parameterized as $\frac{\mu_S}{\mu_B} \simeq 0.164 + 0.018\sqrt{s_{NN}}$. We have checked that the value of T and μ_B obtained using the yields extrapolated to 4π or from midrapidity measurements, have little impact on our study. However in order to study the rapidity (y) dependence, the μ_B parameterizations $\mu_B = 0.024 + 0.011y^2$ and $\mu_B = 0.237 + 0.011y^2$ at $\sqrt{s_{NN}} = 200$ GeV [17] and $\sqrt{s_{NN}} = 17.3$ GeV [18], respectively are used in the calculations.

3. Results

3.1. Kinematic acceptance in η and p_T

Figure 1 shows the variation of $\chi^{(3)}_x/\chi^{(2)}_x$ and $\chi^{(4)}_x/\chi^{(2)}_x$ as a function of η acceptance for $\sqrt{s_{NN}} = 200$ GeV and $\sqrt{s_{NN}} = 17.3$ GeV. Where x stands for either net-baryon (B) (Fig. 1 (a) and (b)), net-charge (Q) (Fig. 1 (c) and (d)), or net-strangeness (S) (Fig. 1 (e) and (f)). For each beam energy we show the effect of considering HRG parameters (μ, T) fixed to parameterization based on midrapidity data and also a parameterization based on the η dependent value of (μ, T). The difference between the two cases are small. For the subsequent studies we only present results for different $\sqrt{s_{\rm NN}}$ using the parameterization of the chemical freeze-out parameters based on the measurement of particle yields at midrapidity. A clear dependence of $\chi^{(3)}_x/\chi^{(2)}_x$ and $\chi^{(4)}_x/\chi^{(2)}_x$ on η acceptance is observed for net-charge (Fig. 1 (c) and (d)) and net-strangeness (Fig. 1 (e) and (f)). The $\chi^{(3)}_B/\chi^{(2)}_B$ and $\chi^{(4)}_B/\chi^{(2)}_B$ values (Fig. 1 (a) and (b)) are however found to be independent of η acceptance for the two beam energies studied. This underscores the need to carefully consider η acceptance effects when comparing HRG model results to experimental data, especially for net-charge and net-strangeness fluctuation measures.

Figure 2 shows the variation of $\chi^{(3)}_x/\chi^{(2)}_x$ and $\chi^{(4)}_x/\chi^{(2)}_x$ as a function of $\sqrt{s_{\rm NN}}$ for various p_T acceptances. The choice of these particular values of p_T acceptance ranges are motivated by existence of the corresponding experimental measurements [5, 12, 13]. It is observed that $\chi^{(3)}_x/\chi^{(2)}_x$ and $\chi^{(4)}_x/\chi^{(2)}_x$ have a clear p_T acceptance dependence at all beam energies for net-charge (Fig. 2 (c) and (d)) and net-strangeness (Fig. 2 (e) and

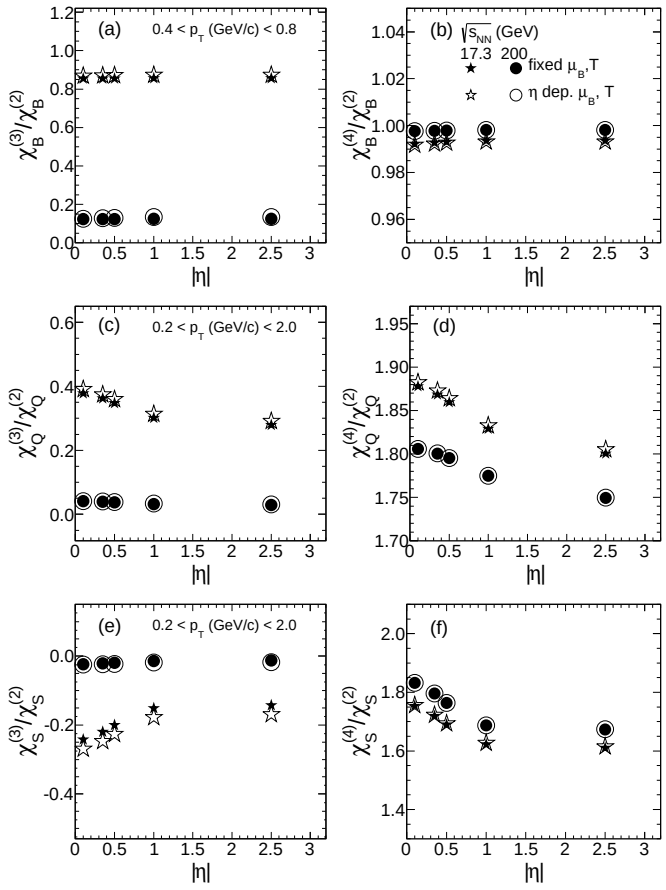

Figure 1: The η acceptance dependence of $\chi_x^{(3)}/\chi_x^{(2)}$ and $\chi_x^{(4)}/\chi_x^{(2)}$ for two different beam energies. In panel (a) and (b) x = net-baryon B, (c) and (d) x = net-charge Q, and in (e) and (f) x = net-strangeness S. Also shown are the results with (labeled "dep.") and without (labeled "fixed") the η dependence of chemical freeze-out parameters μ_B and T.

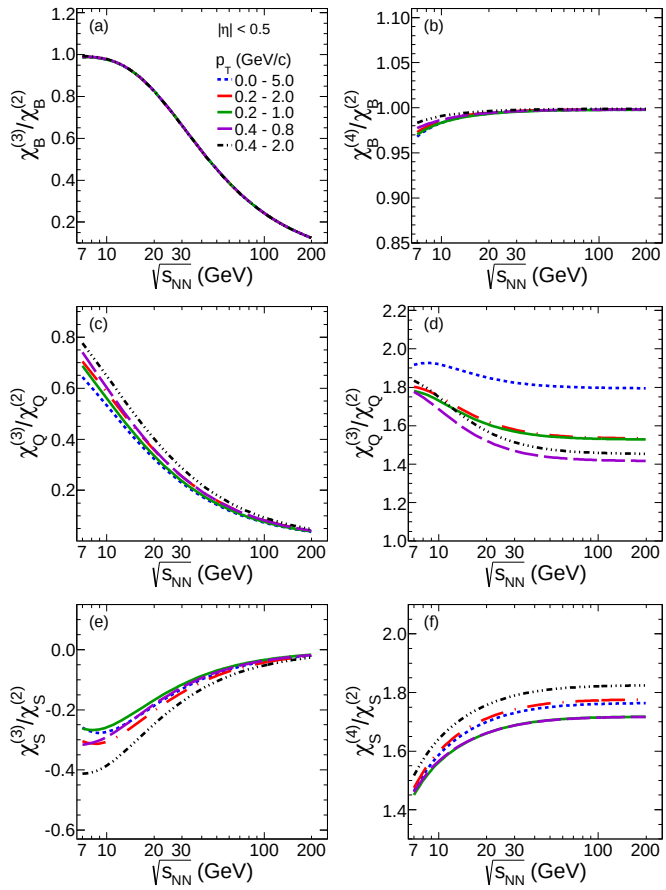

Figure 2: (Color online) The p_T acceptance dependence of $\chi_x^{(3)}/\chi_x^{(2)}$ and $\chi_x^{(4)}/\chi_x^{(2)}$ for different $\sqrt{s_{NN}}$. Where x stands for either net-baryon (B) (panels (a) and (b)), net-charge (Q) (panels (c) and (d)), and net-strangeness (S) (panels (e) and (f)).

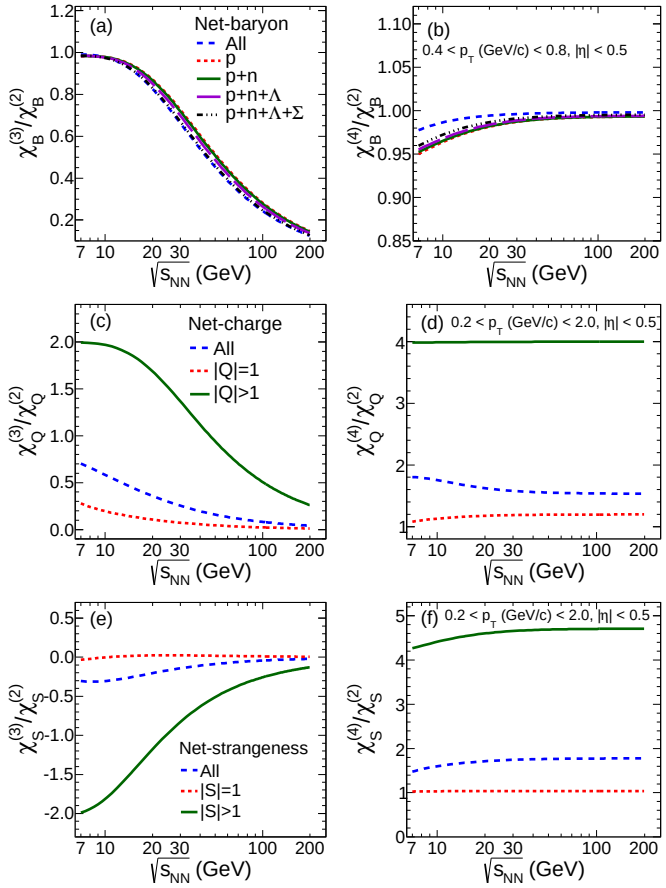

Figure 3: (Color online) The variation of $\chi_x^{(3)}/\chi_x^{(2)}$ and $\chi_x^{(4)}/\chi_x^{(2)}$ for net-baryon (B), net-charge (Q), and net-strangeness (S) as a function of collision energy ($\sqrt{s_{\rm NN}}$). The results are shown for different baryons (panels (a) and (b)), electric charge states (panels (c) and (d)) and strangeness number (panels (e) and (f)) considered in the calculation.

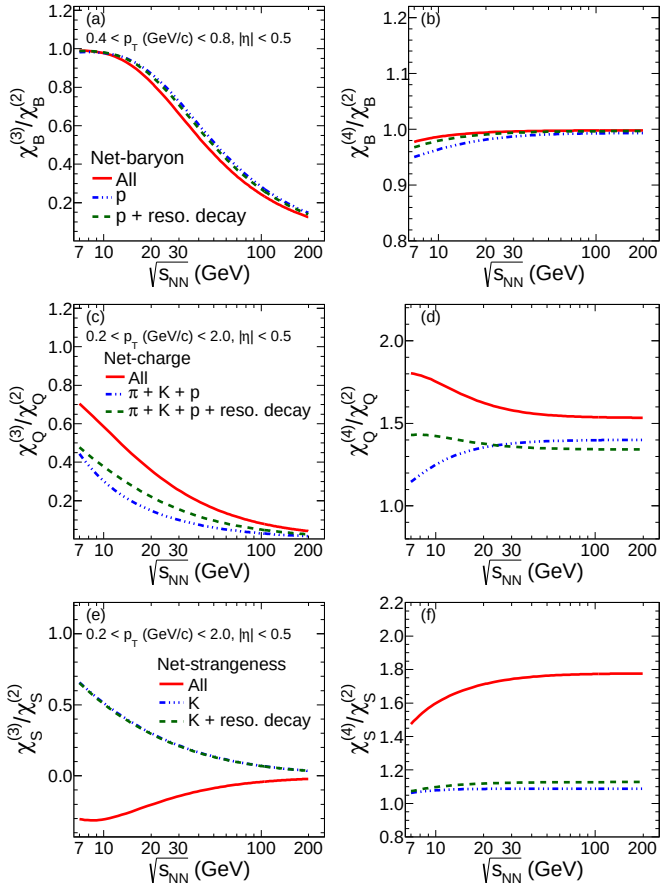

Figure 4: (Color online) The variation of $\chi_x^{(3)}/\chi_x^{(2)}$ and $\chi_x^{(4)}/\chi_x^{(2)}$ for net-baryon (B), net-charge (Q), and net-strangeness (S) with different beam energies ($\sqrt{s_{\rm NN}}$) with and without resonance decay daughter particle acceptance effects.

(f)). However the p_T acceptance dependences for net-baryon (Fig. 2 (a) and (b)) is substantially weaker. Hence the p_T acceptance study also emphasizes the need to consider the actual experimental acceptance for model comparisons in fluctuation measures. At the same time both the kinematic acceptance studies in η and p_T shows net-baryon fluctuation measures are least affected.

3.2. Conserved charge states

Figure 3 shows the variation of $\chi_x^{(3)}/\chi_x^{(2)}$ and $\chi_x^{(4)}/\chi_x^{(2)}$ as a function of $\sqrt{s_{\rm NN}}$ for various types of baryons (Fig. 3 (a) and (b)), values of electric charge states, $|Q| = 1$ and $|Q| > 1$ (Fig. 3 (c) and (d)), and values of strangeness number, $|S| = 1$ and $|S| > 1$ (Fig. 3 (e) and (f)). For each of the cases the observables are compared to the respective values with inclusion of all conserved charge states and baryons. We find a strong dependence of the $\chi_Q^{(3)}/\chi_Q^{(2)}$ and $\chi_Q^{(4)}/\chi_Q^{(2)}$ on whether we consider $|Q| = 1$ or $|Q| > 1$, both differing from the case of inclusion of all charge states. Same is the situation for net-strangeness. On the other hand, successive inclusion of different baryons, starting with protons seems to have some small effect on the $\chi_B^{(3)}/\chi_B^{(2)}$ and $\chi_B^{(4)}/\chi_B^{(2)}$ values only at the lower beam energies. The absence of baryons with $|B| > 1$ makes the net-baryon number fluctuations more advantageous and less prone to kinematic acceptances as compared to the net-charge or net-strangeness fluctuation measures.

3.3. Resonance decay

In a realistic experimental condition, it is likely to happen that not all the daughter particles of a resonance fall within a given experimental acceptance. This would lead to a different kind of efficiency factor in determining the net-charge, net-strangeness and net-baryon number distributions. For example consider a Δ^{++} which decays to proton and pion. Three possibilities may happen, both the proton and pion could fall within the experimental η and $p_{\rm T}$ acceptances, one of them could fall into the acceptance or none of them could fall into the acceptance. These cases will contribute differently to the corresponding measured net-charge and net-proton distributions.

We have studied this effect in the following manner. The conventional way to incorporate resonance decay is to use the definition [19],

$$\langle N_i \rangle = \langle N_i^* \rangle + \sum_R \langle N_R \rangle \langle n_i \rangle_R, \quad (5)$$

where N_i^* is the primordial yield of the i^{th} hadron species, N_R is the contribution from resonance decay, the summation $\sum_R$ runs over all types of resonances and $\langle n_i \rangle_R = \sum_r b_r^R n_{ir}^R$, with n_{ir} being the number of particles contributing to the i^{th} species via the decay mode r of the resonance R and b_r^R is the corresponding branching ratio. The $< n_i >$ can be interpreted as a type of efficiency (ϵ_R) correction to the contribution coming from the resonance decay. Where $\epsilon_R = 1$ in the absence of any kinematic cuts. The particle yields then can be written as $\langle N \rangle = \sum_i \langle N \rangle_i + \sum_R \epsilon_R \langle N_R \rangle$. Assuming that the resonance yields follow a Poisson distribution, the mean of the distribution can be corrected by factor ϵ_R and the same correction factor can be applied for rest of the cummulants. If N is the number of resonances and n is the number that survives the experimental acceptance, then $\epsilon_R = b_r^R n/xN$, where x is the conserved charge = B, Q or S. We have used ϵ_R like an efficiency correction factor while computing the susceptibilities as given in equations 3 and 4. The results of $\chi_x^{(3)}/\chi_x^{(2)}$ and $\chi_x^{(4)}/\chi_x^{(2)}$ with and without considering the effect of resonance daughter particle acceptances are shown in Fig. 4. In Fig. 4(a) and (b), three cases for $\chi_B^{(3)}/\chi_B^{(2)}$ and $\chi_B^{(4)}/\chi_B^{(2)}$ are shown within a realistic acceptance of $|\eta| < 0.5$ and $0.4 < p_T < 0.8$ GeV/c. The results for all baryons without any resonance decay (solid red curve), results for protons without any resonance decay contribution (dotted blue curve) and results for protons with resonance decay (dashed green curve). Similarly in Fig. 4(c) and (d) shows $\chi_Q^{(3)}/\chi_Q^{(2)}$ and $\chi_Q^{(4)}/\chi_Q^{(2)}$ respectively, for all charges without resonance decay (solid red curve), pion, kaon and protons without resonance decay (dotted blue curve) and pion, kaon and protons with resonance decay (dashed green curve). Fig. 4(e) and (f), are shown the results for all strangeness without resonance decay (solid red curve), kaons without resonance decay (dotted blue curve) and kaons with resonance decay (dashed green curve). As one can see from the figure, the resonance decays certainly affect all of the ratios. The effects of acceptance of resonance decay daughters are large for net-charge and net-strangeness compared to net-baryons. The acceptance used in this analysis are modest and are close to the present experimental scenario.

Through our work we have emphasized the need for considering experimental acceptances of various kinds in model, such as HRG, before they are considered to provide the baseline to experimental measurements for drawing physics conclusions. Hence in the Tables 1, 2, 3,and 4 we provide values of $\chi_x^{(3)}/\chi_x^{(2)}$ and $\chi_x^{(4)}/\chi_x^{(2)}$ for typical ongoing experimental acceptances. The $\chi_Q^{(3)}/\chi_Q^{(2)}$ and $\chi_Q^{(4)}/\chi_Q^{(2)}$ values are provided for two typical acceptances $|\eta| < 0.5$, $0.2 < p_T < 2.0$ GeV/c and $|\eta| < 0.35$, $0.3 < p_T < 1.0$ GeV/c (Table 1 and Table 2). The $\chi_S^{(3)}/\chi_S^{(2)}$ and $\chi_S^{(4)}/\chi_S^{(2)}$ are provided for a typical acceptance of $|\eta| < 0.5$, $0.2 < p_T < 2.0$ GeV/c (Table 3). The $\chi_B^{(3)}/\chi_B^{(2)}$ and $\chi_B^{(4)}/\chi_B^{(2)}$ are provided for a typical acceptance of $|\eta| < 0.5$, $0.4 < p_T < 0.8$ GeV/c (Table 4).

4. Summary

In summary, using a hadron resonance gas model we have studied the effect of limited experimental acceptance on observables like n^{th} order susceptibilities $\chi_x^{(n)}$, associated with con-

Table 1: **Ratios of the moments for net-charge within $|\eta| < 0.5$, and $0.2 < p_T < 2.0$ GeV/c**

$\sqrt{s_{NN}}$	$\chi_Q^{(3)}/\chi_Q^{(2)}$	$\chi_Q^{(4)}/\chi_Q^{(2)}$
5	0.526	1.413
7.7	0.414	1.430
11.5	0.321	1.407
15	0.265	1.390
19.6	0.215	1.375
27	0.165	1.361
39	0.119	1.352
62.4	0.077	1.346
130	0.038	1.343
200	0.025	1.342
2760	0.002	1.341

Table 2: **Ratios of the moments for net-charge within $|\eta| < 0.35$, and $0.3 < p_T < 1.0$ GeV/c**

$\sqrt{s_{NN}}$	$\chi_Q^{(3)}/\chi_Q^{(2)}$	$\chi_Q^{(4)}/\chi_Q^{(2)}$
5	0.432	1.231
7.7	0.332	1.245
11.5	0.256	1.233
15	0.212	1.222
19.6	0.172	1.213
27	0.132	1.205
39	0.095	1.199
62.4	0.062	1.196
130	0.031	1.194
200	0.020	1.193
2760	0.001	1.193

Table 3: **Ratios of the moments for net-Kaon within $|\eta| < 0.5$, and $0.2 < p_T < 2.0$ GeV/c**

$\sqrt{s_{NN}}$	$\chi_K^{(3)}/\chi_K^{(2)}$	$\chi_K^{(4)}/\chi_K^{(2)}$
5	0.726	1.058
7.7	0.560	1.090
11.5	0.428	1.108
15	0.353	1.115
19.6	0.288	1.120
27	0.222	1.123
39	0.162	1.125
62.4	0.107	1.127
130	0.054	1.128
200	0.035	1.128
2760	0.003	1.128

Table 4: **Ratios of the moments for net-proton within $|\eta| < 0.5$, and $0.4 < p_T < 0.8$ GeV/c.**

$\sqrt{s_{NN}}$	$\chi_p^{(3)}/\chi_p^{(2)}$	$\chi_p^{(4)}/\chi_p^{(2)}$
5	0.981	0.961
7.7	0.987	0.975
11.5	0.962	0.984
15	0.920	0.988
19.6	0.851	0.991
27	0.737	0.993
39	0.586	0.995
62.4	0.407	0.996
130	0.210	0.997
200	0.139	0.997
2760	0.010	0.997

served quantities like net-charge ($x = Q$), net-strangeness ($x = S$) and net-baryon number ($x = B$). The various order susceptibilities which can also be calculated in QCD based models are related to the moments (σ, S and κ) of the corresponding measured conserved number distributions. These observables have been widely used to understand the freeze-out conditions in heavy-ion collisions and various aspects of the phase structure of the QCD phase diagram. Our study demonstrates the importance of considering experimental acceptances of different kinds before measurements are compared to theoretical calculations, specifically in the use of HRG model as a baseline for such fluctuation based study. We observe finite kinematic acceptances in η and p_T have a strong effect on the $\chi_Q^{(n)}$ and $\chi_S^{(n)}$ values. These susceptibilities are also very sensitive to the accepted electric charge states and strangeness states in the experiment. In addition we find in this model the $\chi_Q^{(n)}$ and $\chi_S^{(n)}$ values depends on the experimental acceptance of the decay daughters from various resonances produced in high energy heavy-ion collisions. Within this model and the kinematic regions used in the our study, we find that the dependence on acceptance and resonance decays are stronger for both net-charge and net-strangeness compared to that of net-baryons.

Acknowledgments BM is supported by the DST Swarna-Jayanti project fellowship. PG acknowledges the financial support from CSIR, New Delhi, India.

References

[1] S. Gupta, X. Luo, B. Mohanty, H. G. Ritter and N. Xu, Science **332** (2011) 1525 [arXiv:1105.3934 [hep-ph]].
[2] R. V. Gavai and S. Gupta, Phys. Lett. B **696** (2011) 459 [arXiv:1001.3796 [hep-lat]].
[3] F. Karsch and K. Redlich, Phys. Lett. B **695** (2011) 136 [arXiv:1007.2581 [hep-ph]].
[4] A. Bazavov, H. T. Ding, P. Hegde, O. Kaczmarek, F. Karsch, E. Laermann, S. Mukherjee and P. Petreczky *et al.*, Phys. Rev. Lett. **109** (2012) 192302 [arXiv:1208.1220 [hep-lat]].
[5] M. M. Aggarwal *et al.* [STAR Collaboration], Phys. Rev. Lett. **105** (2010) 022302 [arXiv:1004.4959 [nucl-ex]].
[6] M. A. Stephanov, Phys. Rev. Lett. **107** (2011) 052301 [arXiv:1104.1627 [hep-ph]].
[7] P. Braun-Munzinger, B. Friman, F. Karsch, K. Redlich and V. Skokov, Phys. Rev. C **84** (2011) 064911 [arXiv:1107.4267 [hep-ph]].
[8] B. Friman, F. Karsch, K. Redlich and V. Skokov, Eur. Phys. J. C **71** (2011) 1694 [arXiv:1103.3511 [hep-ph]].
[9] C. B. Yang and X. Wang, Phys. Rev. C **84** (2011) 064908 [arXiv:1107.4740 [nucl-th]].
[10] M. Asakawa, S. Ejiri and M. Kitazawa, Phys. Rev. Lett. **103** (2009) 262301 [arXiv:0904.2089 [nucl-th]].
[11] P. Braun-Munzinger, K. Redlich and J. Stachel, In *Hwa, R.C. (ed.) et al.: Quark gluon plasma* 491-599 [nucl-th/0304013].
[12] D. McDonald [STAR Collaboration], arXiv:1210.7023 [nucl-ex].
[13] J. T. Mitchell [PHENIX Collaboration], arXiv:1211.6139 [nucl-ex].
[14] J. Cleymans, H. Oeschler, K. Redlich and S. Wheaton, Phys. Rev. C **73** (2006) 034905 [hep-ph/0511094].
[15] F. Becattini, J. Cleymans, A. Keranen, ESuhonen and K. Redlich, Phys. Rev. C **64** (2001) 024901 [hep-ph/0002267].
[16] A. Andronic, P. Braun-Munzinger and J. Stachel, Nucl. Phys. A **772** (2006) 167 [nucl-th/0511071].
[17] J. Cleymans, J. Phys. G: Nucl. Part. Phys. **35** (2008) 044017.
[18] F. Becattini, J. Cleymans and J. Strumpfer, PoS CPOD **07** (2007) 012 [arXiv:0709.2599 [hep-ph]].
[19] J. Fu, Phys. Lett. B (in press).